Modeling Activity of Neurons from NRG recording study

Introduction

Humans and other primates use combinations of eye and head movements to move the line of sight. Depending on the behavioral task, different types of movements may be employed. Gaze shifts are used to quickly acquire a new target using a rapid head rotation combined with a saccadic eye movement. Gaze pursuit can be used to follow a moving target and combines head rotation with smooth pursuit eye movements. These behaviors are often used in combination to efficiently view objects of interest within the natural world.

Investigations of the neural correlates of these behaviors reveal that separate neural mechanisms are employed. The superior colliculus (SC) is a key structure in the control of gaze shifts. Experimental evidence demonstrates that the SC contains an organized motor map that represents a desired gaze displacement signal used to generate gaze shifts. No analogous organized structure has been identified for pursuit movements. Instead, pursuit seems to be controlled by a reciprocal cerebro-ponto-cerebellar circuit. This circuit includes areas of visual motion processing and the frontal eye fields in the cortex, pontine nuclei that relay these signals to the cerebellum and follicular neurons, which are likely to be responsible for generating smooth pursuit eye movements. Although there is evidence of gaze-related signals at each stage in this circuit, it has not been demonstrated that these commands are used to generate head movements during pursuit.

The identification of brain regions responsible for dissociating gaze signals into the appropriate eye and head motor commands is an ongoing scientific pursuit. The technique of restraining the head has allowed researchers to understand the pathways driving eye and gaze movements, but does not distinguish between the two. When the head is free to move, behavioral paradigms can be employed to dissociate gaze from eye-related signals. This, combined with head-restrained studies, has allowed for significant progress in the mapping of the oculomotor premotor circuits. A similar method can be used to map the premotor circuits responsible for driving head movements.

Anatomic evidence exists for the neurophysiologic basis of head control in gaze shifts. In particular, some neurons in the reticular formation receive inputs from the SC and project to motor neurons in the cervical spinal cord. This places them in the ideal location to transform gaze displacement signals from the SC into appropriate head motor commands, though the activity of these neurons has not been described in primates performing head-unrestrained movements.

Recordings from the medullary and pontine reticular formation in cats have identified some neurons with activity correlated with certain dynamics of head movement. Micro-stimulation of analogous structures in monkeys has been shown to produce movements of the eyes, head, ears, mouth and produce other movements, depending on the region stimulated. Quessy and Freedman investigated a region of NRG that produces ipsilateral horizontal head rotation when stimulated, with kinematics similar to those observed during horizontal gaze shifts. They further demonstrated that while stimulating these regions does not produce eye movement directly, stimulation does alter ongoing eye movements initiated as part of a gaze shift, implying that NRG is part of the circuit used to produce gaze shifts.

In addition to likely gaze-shift-related inputs from the SC, NRG also receives input from many other areas, including motor and prefrontal cortex, the cerebellum and basal ganglia. This diversity of inputs suggests the potential for a greater role for NRG, including the potential for involvement in producing the head movements associated with gaze pursuit. Cats do not employ smooth pursuit movements like humans and monkeys do, so no physiologic evidence exists for the activity of this region during such movements.

In this study, we return to the portion of NRG stimulated by Quessy and Freedman to record the activity of neurons that may be responsible for producing the head movement observed during stimulation. We use established behavioral paradigms to dissociate gaze, eye and head movement during gaze shifts that allow us to identify neurons whose activity is associated with head movement apart from gaze or eye movements. New

techniques for dissociating the gaze, eye and head movements associated with gaze pursuit are also employed, enabling us to identify any neurons involved in producing the head movements associated with pursuit and to determine whether these are a separate population from those involved in producing head movements during gaze shifts. Our behavioral paradigms also allow us to assess neurons for activity related to eye position in the orbits. This is information required to produce a head-specific motor command from gaze-related signals.

Methods

Two rhesus monkeys (*Macaca mulatta*) served as subjects. Two sterile surgeries were performed to prepare each animal for neurophysiological experiments. In the first, a stainless-steel post was affixed to the skull with bone screws, and a teflon-coated coil of wire was implanted under the conjunctiva of one eye (Judge et al. 1980). Following this, the monkeys were trained to perform behavioral tasks. When they became proficient at this tasks, a second surgery was performed to affix a recording chamber over a trephine craniotomy. The chamber was positioned on the midline at stereotaxic zero. All surgical and experimental procedures were approved by the University of Rochester Animal Care and Use Committee and were in compliance with the National Institutes of Health Guide for the Care and Use of Animals.

The data presented in this study were collected concurrently with the behavioral data described in the previous chapter. Therefor, the collection of behavioral data and presentation of visual targets is identical. Briefly, monkeys were placed in a custom-designed primate chair during experiments, that restrained the body but allowed free movement of the head. A small, lightweight cam-lock device was attached to the head. The position of the head was determined by the orientation of coil of Teflon-coated wire attached to the device, using the same method as the implanted search coil. Three red lasers attached to the device allowed behaviral control of initial eye-in-hea position (described in detail in previous chapter).

The monkey chair was placed in the center of a cube containing three pairs of magnetic field coils (CNC Engineering, Seattle, WA). Signals from the gaze and head coils were sampled at 1 kHz and filtered using a five-pole, low-pass Bessel filter with a cutoff frequency of 3 kHz. A second low-pass filter with a time constant of 0.3ms was applied to the signal before digitizing. The current in the coils was linearly related to the horizontal rotational position of the coils in the field within 2 degrees over 360 degrees.

Visual targets were presented on the inner surface of a 1.5 m hemisphere (0.5 in acrylic; Capital Plastics, Beltsville, MD). Two additional red lasers, attached to independent, two-axis-motorized gimbals (RGV 100 rotation stages; Newport, Irvine, CA) presented targets with < 0.01 degree accuracy. An infrared camera allowed the experimenters to view the monkeys, which was particularly useful for assessing head-roll during microstimulation.

Neurophysiology

Single neurons in NRG were isolated using a tungsten micro-electrode (Micro Probes), amplified, filtered and saved for offline analysis. The anterior/posterior position of the electrode in the chamber was chosen using the characteristic firing pattern of the abducens motor nucleus as a landmark. We close electrode tracts that traveled posterior to the nucleus to avoid damaging motor neurons, and continued deeper. On most tracts, the characteristic population bursting for ipsiversive gaze shifts of PPRF was noted, as well as occasional MLBs and LLBNs. Once the electrode was advanced beyond the level of population gaze-shift-related activity, we also characterized the location's response to micro-stimulation. We sought regions that produced horizontal head rotation on stimulation, using the stimulation parameters of Quessy and Freedman (2004) as a guide. Superficial to this region, we observed evoked ear movements as well as head movements with vertical or roll components. Any neurons isolated deep to the level of population gaze activity were recorded as a candidate for inclusion in this study.

Modeling

We are attempting to find a function of the recorded eye and head movements that will predict the firing rate of the neuron during the trial. We convert the recorded spike times into a continuous function by convolving them with a Gaussian with a 15ms standard deviation to create a spike density function. We scale the spike density function so that it approximates the firing rate in spikes per second. For this analysis, we separate leftward and rightward movements to produce 12 possible predictor variables: (right/left)(eye/head)(position/velocity/acceleration), represented by the abbreviations: *rhp, lhp, rep, lep, rhv, lhv, rev, lev, rha, lha, rea* and *lea*.

We use Matlab's **stepwiselm** function, beginning with a constant model. The function evaluates the set of available terms, which includes the predictor variables described above, as well as pairwise interactions. If any of these terms improve the R^2 of the model by 0.05 or more, the threshold criterion we chose, it includes the best term and then repeats the evaluation to see if any other terms could improve the model further. If these neurons were involved in generating the observed eye and head behavior, we assume that there would be a time delay between neural activity and movement. We repeated this step-wise model fitting to shifted data, in 10ms increments up to 200ms. We employed step wise fitting method to find the best fit at each location independently. We then chose the delay that gave the best fit, determined by the R^2 weighted by the number of terms in the model. Each additional term must improve the fit by at least 0.05. For example, if the best fit at a 50ms delay was a model with two terms an R^2 of 0.29, and the best fit at 60ms was a model with three terms and an R^2 of 0.30, we chose the simpler model.

Results

We isolated 163 neurons (94 from S and 69 from U) in NRG while monkeys performed head-unrestrained gaze shifts and gaze pursuit tasks. The activity of 53 of these neurons was recorded based on apparent head-movement-related activity as perceived by the researchers during recording, and isolation was maintained for at least 50 successful trials. The behavior tasks that our monkeys performed provided us with a large variety of head movements to investigate. Controlling initial eye position provided us with examples of pursuit and gaze shifts of similar velocities and amplitudes with varying amounts of head contribution. This provided us with the ability to identify neurons with head-related activity during recording. For offline analysis, we can compare the firing rate of the neurons to the actual head and eye kinematics on a trial-by-trial basis.

Peak Firing Rate and Peak Head Velocity

Based on the observations of the experimenters during recording, we hypothesized that there is a correlation between the firing rate of the neurons and the velocity of head movements. To test this hypothesis, we first investigated the relatioship between the peak firing rate and the peak velocity on each trial for each neuron. We identified cells that have significant correlations between these two variables and fit linear regression models. In figure 1, we show an example cell demonstrating this process. Panel 1A shows the head velocity and corresponding activity of the neuron during a fast, leftward head movement, while 1B shows the same during a slower head movement. For each trial, we record the peak head velocity and the peak firing rate of the neuron, which are plotted in 1C. We fit a linear regression model for the relationship between peak firing rate and peak velocity in each direction. For the example neuron shown in 1C, this regression was significant ($p<0.001$) for leftward movements only. Table 1 summarizes the results of this analysis for each neuron in our population.

We find that 20 cells show a significant regression ($p<0.001$) with rightward movements, 28 for leftward and 14 for both. That is a total of 34 neurons with a significant correlation with head movements of at least one direction. If we impose the additional requirement that firing rate must increase with faster head movements (slope of regression is positive for rightward and negative for leftward head movements, we find 19 for rightward, 23 for leftward and 9 for both; a total of 33 neurons (67%). In figure 2, we plot regression lines for these cells on same axes, as three groups, corresponding to whether they are significant for leftward, rightward or both directions.

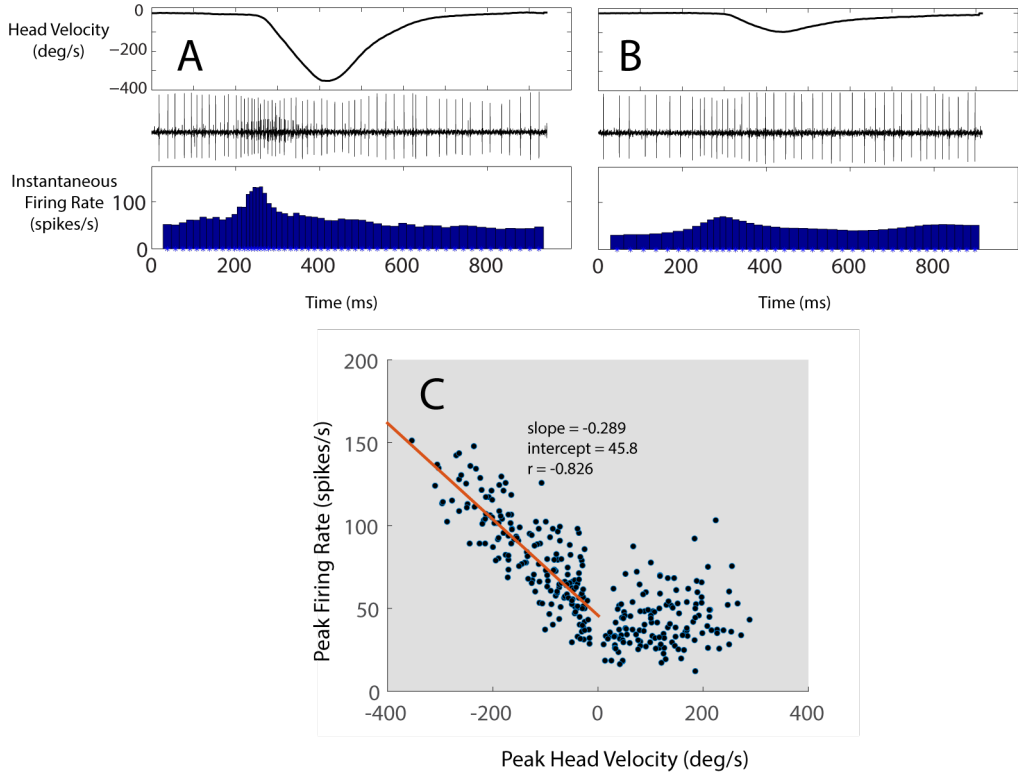

Figure 1: Example of correlation between peak head velocity and peak firing rate.

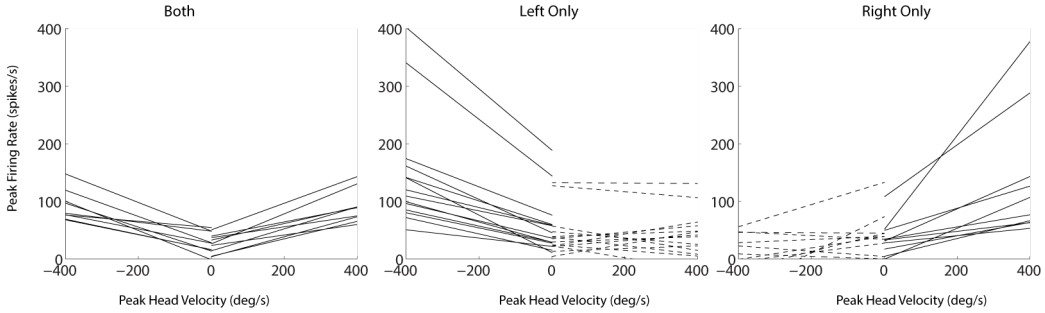

Figure 2: Linear regression models for the relationship between peak head velocity and peak firing rate of each neuron.

Pursuit vs Gaze shift activity One question we sought to answer when designing these experiments regarded whether the neurons in NRG were participating in head movements made during both gaze shifts and pursuit. An alternative is that NRG activity is dependent on SC activity and therefore only active during gaze shifts. General observation did not reveal any neurons with activity limited to only head movements associated with one behavioral task. Despite this, some neurons seemed to fire more rapidly during pursuit movements, even though the head movements were faster.

Eye Position

Observation of the fixation prior to movement initiation indicates position-related firing in several neurons. We use anova to identify cells with significantly different firing rates for the three different combination of eye and head positions in use during fixation. To determine whether this firing is due to eye or head position, we must compare to other parts of the trial, such as at the end of a gaze shift when the eyes are centered and the head is eccentric.

Modeling

The above analysis was restricted to the peak firing rate of the neuron on each trial. Further, it assumes that head velocity is an important factor for each neuron. In this section, we use the unbiased modeling approach described in detail in *Methods*. For 51 of the 53 neurons included in this study, we were able to model firing rate as a function of eye or head position, velocity or acceleration. For the neurons we were unable to fit, this means that no individual term improved the variance accounted for (R^2) of the constant model by 0.05 or better, suggesting that these neurons do not have activity related to eye or head movements. The table below shows the shift (the delay between cell activity and the eye and head paramters being modeled), the R^2 indicating goodness of fit, and the formula. Although we allowed for interaction terms in our step-wise fitting procedure, we do not observe interactions.

The histogram below shows the distribution the shifts obtained with this method. The shift represents the separation between the firing rate of the neuron and the eye and head behavior. We hypothesize that this is approximately the latency between the activity and the movements being generated by the activity, but only for cells that are actually involved in generating these movements. The average shift was 95.47ms, with a standard deviation of 47.25.

The next histogram (below), summarizes how well the models fit the activity of the neurons. The average R^2 was 0.29, with a standard deviation of 0.17.

From the above table, it is clear that several different models were found to best describe the neurons in our population. The histogram below indicates how often each particular model appears in our data set.

From this analysis, it appears that many different models are used, but there is a lot of similarity.

```
## stat_bin: binwidth defaulted to range/30. Use 'binwidth = x' to adjust this.
## stat_bin: binwidth defaulted to range/30. Use 'binwidth = x' to adjust this.
## stat_bin: binwidth defaulted to range/30. Use 'binwidth = x' to adjust this.
## stat_bin: binwidth defaulted to range/30. Use 'binwidth = x' to adjust this.
## stat_bin: binwidth defaulted to range/30. Use 'binwidth = x' to adjust this.
## stat_bin: binwidth defaulted to range/30. Use 'binwidth = x' to adjust this.
```

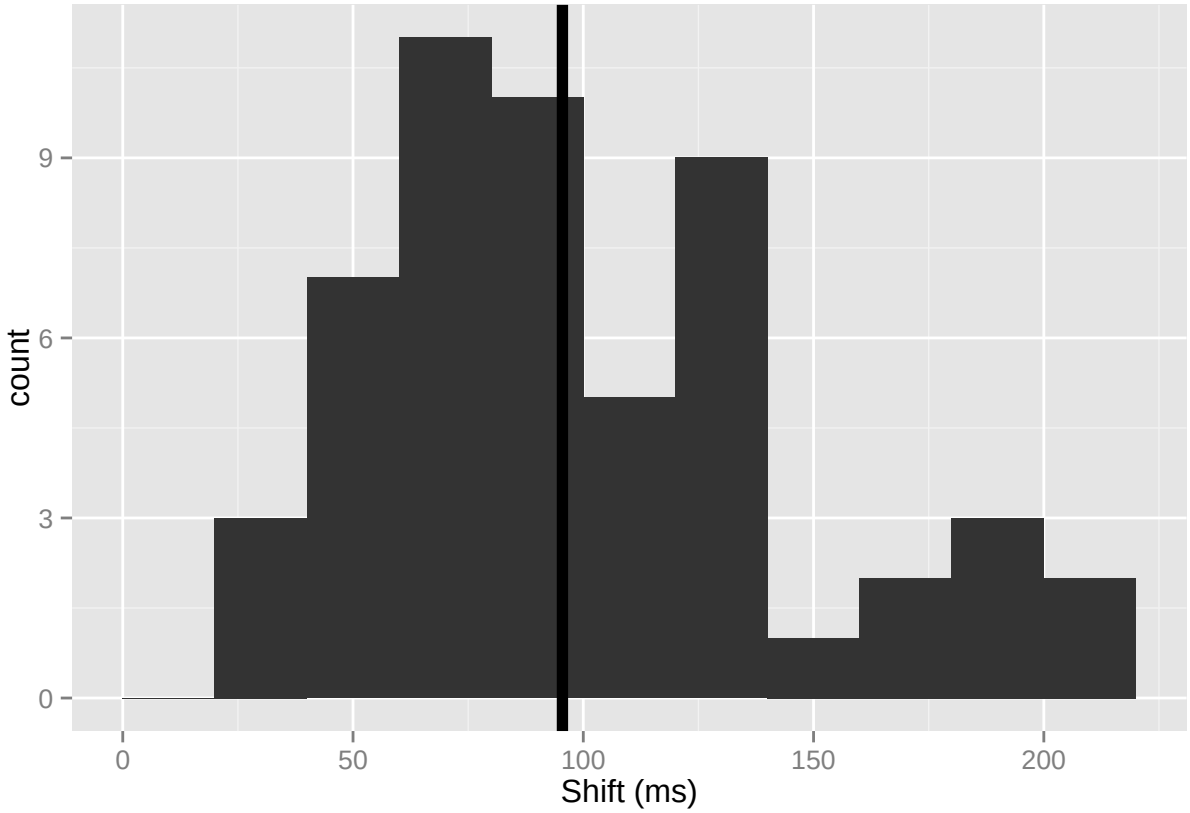

Figure 3: This figure shows a histogram of the distribution of shifts (in ms) found in our modeling procedure.

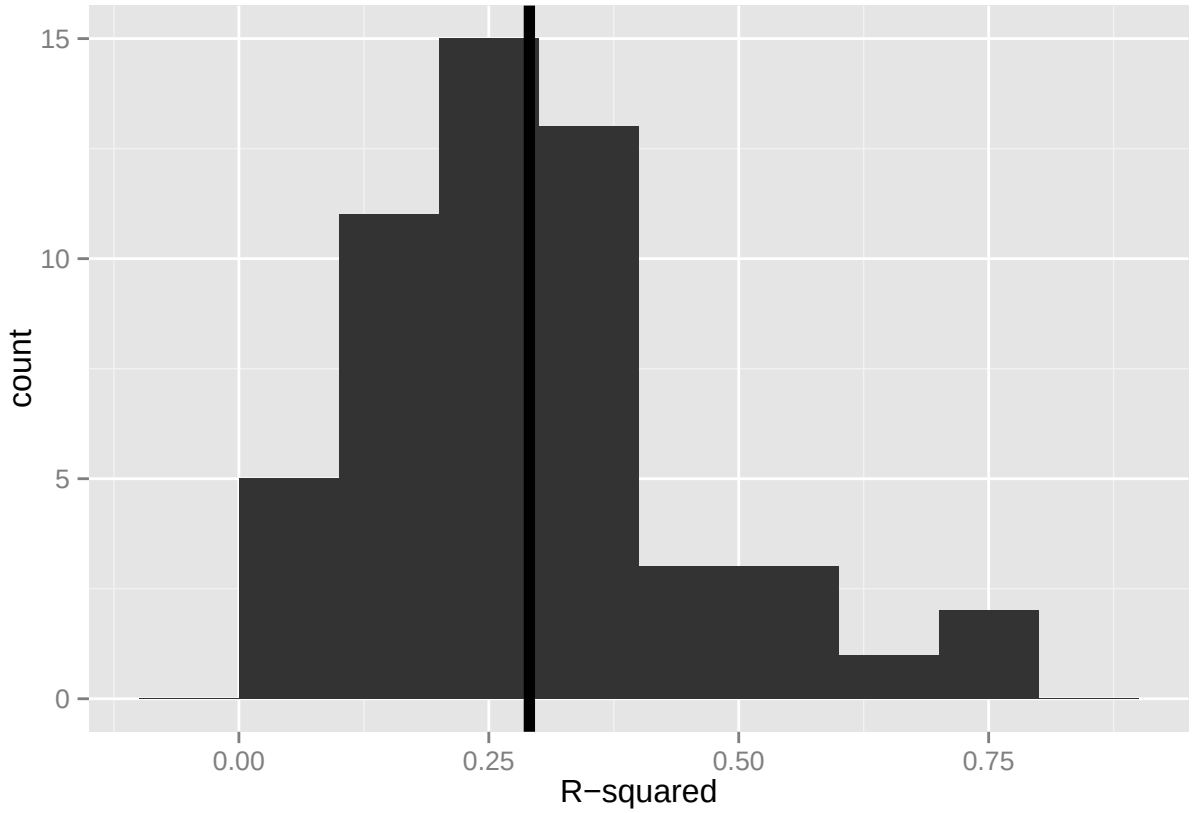

Figure 4:

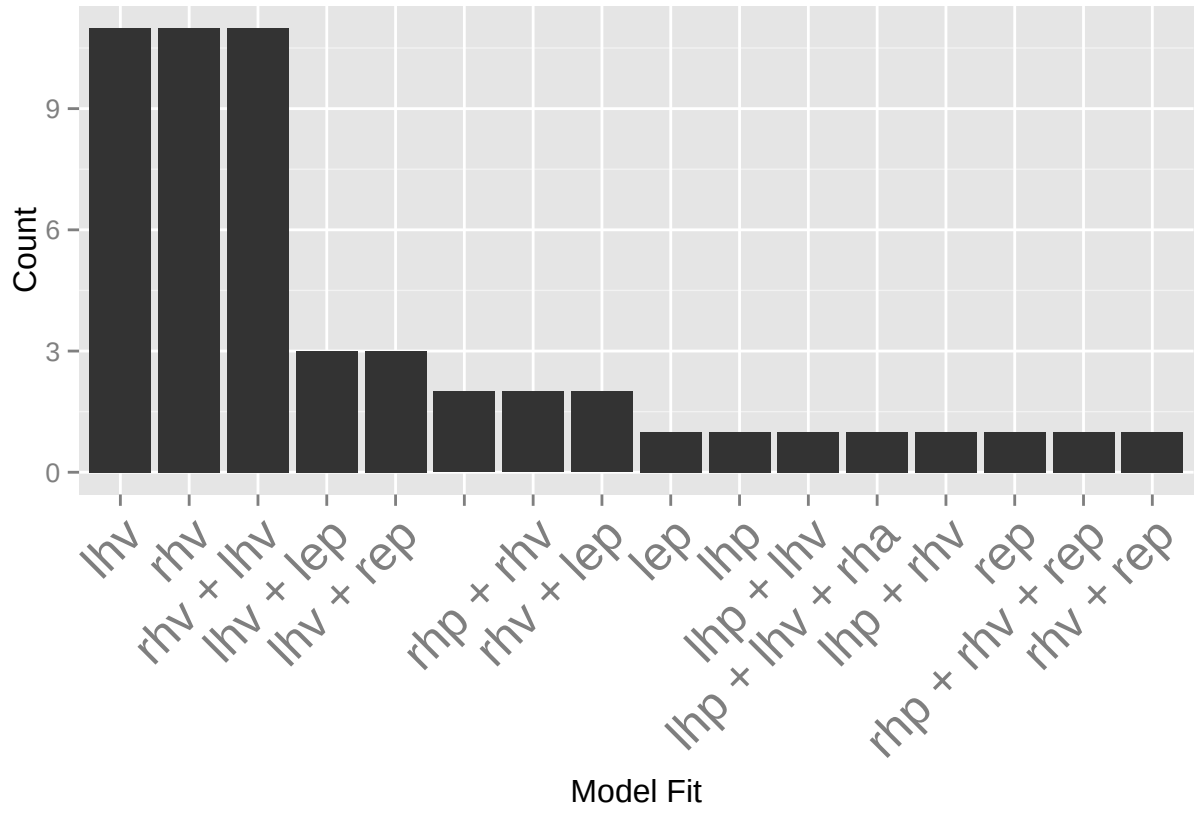
Count
9
6
3
0
lhv
rhv
rhv + lhv
lhv + lep
lhv + rep
rhp + rhv
rhv + lep
lep
lhp
lhp + lhv
lhp + lhv + rha
lhp + rhv
rep
rhp + rhv + rep
rhv + rep
Model Fit

Figure 5:

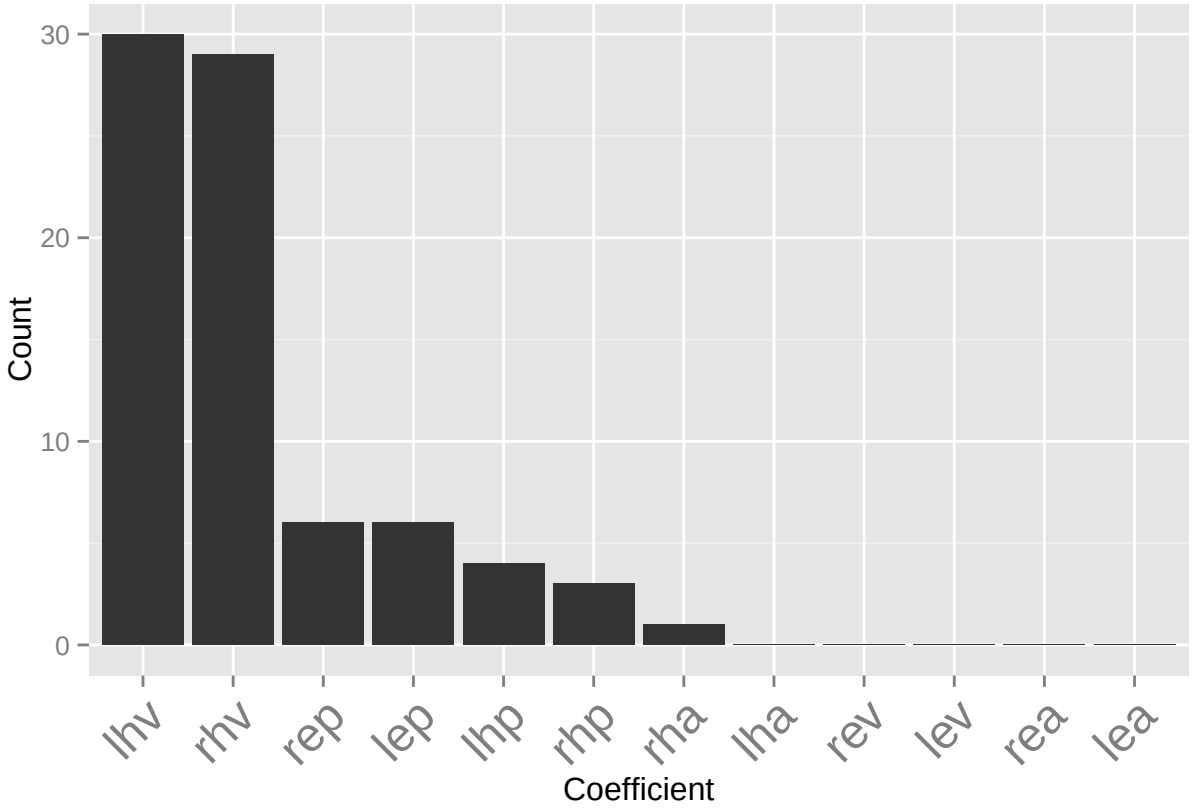
30
20
10
0
Count
lhv
rhv
rep
lep
lhp
rhp
rha
lha
rev
lev
rea
lea
Coefficient

Figure 6:

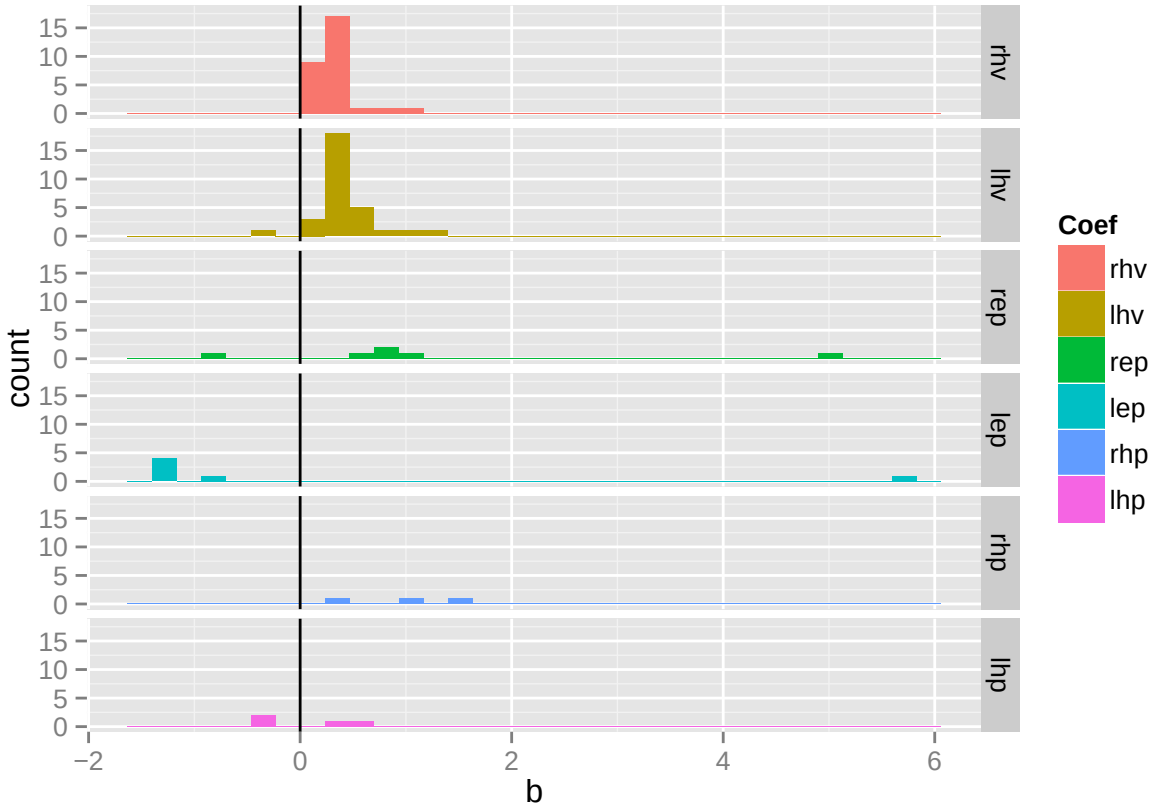

Figure 7:

	Neuron	n.r	slope.r	intercept.r	r.r	p.r	n.l	slope.l	intercept.l	r.l	p.l
1	SB10Jan12	110	0.13	38.80	0.31	0.00	143	-0.10	43.78	-0.32	0.00
2	SC12Dec11	133	0.08	35.22	0.34	0.00	151	-0.32	36.80	-0.81	0.00
3	SD04Jan12	287	0.10	20.67	0.27	0.00	283	-0.12	15.75	-0.49	0.00
4	SD21Sep11	114	0.19	23.82	0.50	0.00	180	-0.11	41.77	-0.51	0.00
5	UB22may12	66	0.16	17.01	0.81	0.00	60	-0.19	16.10	-0.83	0.00
6	UB23mar12	66	0.17	-1.19	0.66	0.00	55	-0.16	20.32	-0.73	0.00
7	UB24oct11	121	0.11	38.84	0.39	0.00	97	-0.10	32.30	-0.41	0.00
8	UC17feb12	364	0.18	-4.48	0.65	0.00	141	-0.26	-7.50	-0.85	0.00
9	SB10Oct11	223	0.47	102.25	0.62	0.00	170	0.14	37.19	0.46	0.00
10	SB21Oct11	94	1.09	4.07	0.84	0.00	63	0.35	70.90	0.53	0.00
11	SC14Oct11	168	0.06	28.64	0.29	0.00	121	0.09	27.00	0.37	0.00
12	SC18Oct11	181	0.40	15.93	0.52	0.00	133	0.12	33.42	0.48	0.00
13	UD16sep11	133	-0.07	25.27	-0.32	0.00	194	-0.17	50.48	-0.40	0.00
14	SB16Sep11	45	0.12	-0.72	0.33	0.03	64	-0.23	16.32	-0.74	0.00
15	SB19Jan12	116	0.16	2.51	0.62	0.00	87	-0.05	4.36	-0.19	0.07
16	SB28Sep11	75	0.42	25.60	0.53	0.00	39	0.08	54.22	0.08	0.63
17	SC07Oct11	103	0.15	35.73	0.21	0.03	78	-0.17	32.85	-0.57	0.00
18	SC21Dec11	140	0.09	34.86	0.24	0.00	183	-0.30	41.31	-0.68	0.00
19	SC23Sep11	67	-0.05	41.82	-0.18	0.13	163	-0.20	78.57	-0.39	0.00
20	SD03Nov11	111	0.40	-18.97	0.41	0.00	132	0.39	175.69	0.24	0.01
21	SD09Jan12	104	-0.14	55.26	-0.28	0.00	156	-0.51	131.46	-0.31	0.00
22	SD13Jan12	90	0.01	145.90	0.00	0.97	158	-0.62	201.51	-0.35	0.00
23	UB05jan12	201	0.28	28.74	0.56	0.00	244	-0.03	64.31	-0.07	0.27
24	UB07oct11	94	0.41	44.05	0.48	0.00	95	-0.29	45.23	-0.27	0.01
25	UB11jan12	56	0.16	71.32	0.20	0.14	95	-0.41	33.07	-0.39	0.00
26	UB16feb12	258	-0.02	11.41	-0.15	0.02	97	-0.18	50.08	-0.45	0.00
27	UB26mar12	199	0.11	28.30	0.12	0.08	157	-0.20	20.82	-0.54	0.00
28	UE31oct11	39	0.06	17.70	0.55	0.00	27	-0.24	10.85	-0.47	0.01
29	SB05Oct11	138	0.03	50.95	0.05	0.56	92	-0.06	48.56	-0.15	0.14
30	SB07Oct11	38	0.09	36.03	0.22	0.18	33	0.01	28.60	0.04	0.83
31	SB15Sep11	57	0.14	19.44	0.31	0.02	45	-0.01	-0.26	-0.19	0.21
32	SB18Oct11	48	0.04	62.02	0.07	0.65	44	-0.02	24.24	-0.08	0.60
33	SB30Sep11	114	0.26	5.34	0.24	0.01	82	-0.05	-0.50	-0.22	0.05
34	SC19Jan12	76	-0.09	20.39	-0.32	0.01	151	-0.12	20.49	-0.13	0.10
35	SC19Oct11	65	0.05	30.30	0.27	0.03	44	-0.03	19.61	-0.07	0.65
36	SC28Nov11	199	0.10	22.35	0.21	0.00	171	0.01	50.18	0.01	0.85
37	SD06Dec11	109	0.03	64.29	0.02	0.81	74	-0.46	45.14	-0.23	0.05
38	SD28Sep11	89	0.01	29.83	0.07	0.51	64	-0.04	17.27	-0.25	0.05
39	SD30Sep11	103	0.08	301.71	0.05	0.62	67	-0.37	110.74	-0.22	0.08
40	SE17Oct11	59	0.14	48.52	0.34	0.01	45	0.05	10.66	0.31	0.04
41	UB04nov11	68	0.08	39.97	0.22	0.07	54	-0.00	35.97	-0.01	0.96
42	UC03jan12	24	0.10	27.95	0.28	0.19	74	-0.05	65.04	-0.05	0.67

Table 1: Results of linear regression modeling between peak head velocity and peak firing rate of each neuron.

	Neuron	shift	rsquared	f
1	SB21Oct11	120	0.77	fr ~ 1 + rhv + rep
2	UB21dec11	60	0.70	fr ~ 1 + lep
3	UB22may12	70	0.64	fr ~ 1 + rhv + lhv
4	SE17Oct11	150	0.58	fr ~ 1 + rhv
5	SB10Oct11	170	0.58	fr ~ 1 + rhp + rhv
6	UC22may12	80	0.57	fr ~ 1 + rhv + lhv
7	SC23Sep11	130	0.47	fr ~ 1 + lhv
8	UBA4jun12	90	0.46	fr ~ 1 + rhv + lhv
9	SD09Jan12	130	0.41	fr ~ 1 + lhv
10	UB23mar12	80	0.40	fr ~ 1 + lhv + rep
11	SC12Dec11	70	0.40	fr ~ 1 + lhv
12	UB16feb12	90	0.40	fr ~ 1 + lhv
13	UB05jan12	60	0.39	fr ~ 1 + lhp + lhv + rha
14	SB15Sep11	110	0.37	fr ~ 1 + rhv
15	UB28sep11	20	0.35	fr ~ 1 + rhp + rhv + rep
16	SD03Nov11	160	0.34	fr ~ 1 + lhv
17	SC18Oct11	40	0.33	fr ~ 1 + rhv + lep
18	SB16Sep11	70	0.32	fr ~ 1 + lhv
19	UD16sep11	130	0.32	fr ~ 1 + lhv
20	UB04nov11	70	0.31	fr ~ 1 + rhv + lhv

Table 2: This table shows the results of a step-wise fitting procedure that with a threshold for inclusion of an increase of 0.5 in the R2